ЖЭТФ, 2010, том 138, вып. 3 (9), стр. 449–468

STEPWISE COMPUTATIONAL SYNTHESIS OF FULLERENE C_{60} DERIVATIVES. FLUORINATED FULLERENES $C_{60}F_{2k}$

E. F. Sheka[*]

General Physics Department, Peoples‘ Friendship University of Russia
117198, Moscow, Russia

Received January 8, 2010

Reactions of fullerene C_{60} with atomic fluorine are studied by the unrestricted broken spin symmetry Hartree–Fock (UBS HF) approach implemented in semiempirical codes based on the AM1 technique. The calculations are focused on a successive addition of a fluorine atom to the fullerene cage following the indication of the highest chemical susceptibility of the cage atom, which is calculated at each step. The proposed computational synthesis is based on the effectively-unpaired-electron concept of the chemical susceptibility of fullerene atoms. The obtained results are analyzed from the standpoints of energy, symmetry, and the composition abundance. A good fitting of the data to experimental findings proves a creative role of the suggested synthetic methodology.

1. INTRODUCTION

The fluorinated fullerene C_{60} decade, started with the first synthesis in 1991 (see reviews [1–4]) and ended by a generalizing theoretical approach to the characterization of fluorinated fullerenes in 2003 [5], without a doubt is one of the best examples of the power and ability of modern chemistry to produce, characterize, and describe a new family of fascinating chemicals at a microscopic level. This is especially impressive because the number of species hidden under the general formula $C_{60}F_{2k}$ (with $k = 1, \ldots, 30$), is definitely countless if all possible isomers at each particular k are taken into account. The first breakthrough in the problem was achieved by experimentalists who showed that 1) only species with an even number of fluorine atoms can be observed, 2) not all $k = 1, \ldots, 30$ fluorinated products but only a restricted set of them can be produced and identified in practice, and 3) a very limited number of isomers, from one to three, are revealed. Products with chemical formulas $C_{60}F_{18}$, $C_{60}F_{36}$, and $C_{60}F_{48}$ dominate in the production list, while minor products from $C_{60}F_2$ to $C_{60}F_{20}$ have also been identified [6]. Mass spectrometry, IR, ^{19}F, and ^{3}He NMR spectroscopy manifested themselves as reliable constituents of a convincing analytical platform for identification of the species.

At the same time, quantum chemical simulations have faced the manyfold isomerism problem in the full measure. Thus, to suggest a convincing atomistic structure of the products produced experimentally, one to three isomers [6] must be chosen among 600 873 146 368 170 isomers of $C_{60}F_{36}$ [7] and 23 322 797 475 isomers of $C_{60}F_{48}$ [7]. To make computations feasible the isomer number must be restricted to unity. Obviously, this might be possible if some global regularities, which govern the fluorination process, can be exhibited. To proceed along this way, it was necessary to answer the following questions.

1. To what kind of chemical reactions does the fullerene fluorination belong?
2. What is the pathway for fluorination of fullerene C_{60}, and does the fluorination of $C_{60}F_2$, e. g., to $C_{60}F_{48}$ follow a single pathway and in regular steps?
3. How can the target carbon atoms of the fullerene cage be chosen prior to any subsequent step of fluorination?
4. How can these measures restrict the number of possible isomers?

In answering the first question, the computing community regarded the fullerene fluorination as a radical reaction [8] of one-by-one addition of fluorine atoms, with the first addition drastically violating the double C–C bond of the fullerene cage and the next addition completing the transformation of the bond into a single one.

Experimental data, particularly a comprehensive study of the electronic structure and chemical bonding

---

[*] E-mail: sheka@icp.ac.ru

of fluorinated fullerenes by X-ray photospectroscopy, near-edge X-ray angular photospectroscopy, UV photospectroscopy, and vacuum-UV absorption [9] give a positive answer to the second question; hence, fluorination of $C_{60}F_2$ to $C_{60}F_{48}$ follows a single pathway and occurs in regular steps.

As regards the choice of target atoms for the subsequent steps, a computing scientist had to solve the dilemma of either accepting the full equality of the fullerene C_{60} atoms with respect to chemical reactivity or seeking regioselectivity of the cage atoms. Obviously, the first option, which has been adopted by the majority of the computational community until now, was absolutely impotent in the solution of the above isomerism problem. Therefore, to proceed with the problem solution, a particular regioselectivity of fullerene atoms has to be accepted. The first suggestion concerns the choice between 6,6 double bonds joining two hexagons and 6,5 single bonds framing pentagons in favor of the former. The next suggestion deals with the separation between carbon sites of the subsequent addition of fluorine atoms either via bonds (1,2-addition, adjacent carbon sites) or via space (1,3- and 1,4-additions, widely spaced carbon sites). It was first proved in [10] that the 1,2-addition is preferable for fluorine. In a decade, the conclusion was confirmed in [5]. The next question concerns the succession of the 1,2-additions. Following a concept of a supposed increase in aromaticity of the fullerene hexagons caused by fluorine addition generalized in [4], a contiguous F_2 addition was suggested with the preference of C–C double bonds adjacent to the prior addition sites.

The above issues are quite important for designing model structures, but they should nevertheless be qualified as general recommendations only. The main problem concerning the number of isomers attributed to each of the $C_{60}F_{2k}$ species is still open. The way out of the situation was suggested in [11], where it was proposed to restrict the number of isomers to those having a three-fold symmetry axis. The proposal was based on a clear experimental evidence of the C_{3v} symmetry of the crown-shaped $C_{60}H_{18}$ species [12]. This has been extended to $C_{60}F_{18}$ [11] and subsequently also to $C_{60}F_{36}$ and $C_{60}F_{48}$ adducts [13–16]. However, under these assumptions, the number of possible isomers is still quite large, e. g., 2695 for $C_{60}F_{36}$ species [17]. The next step toward decreasing the isomer number involved concrete assumptions concerning the molecule symmetry. For example, a crown-shaped structure of $C_{60}F_{18}$ points to the C_{3v} symmetry [11], the consideration of T, C_3, S_6, and D_{3d} structures for $C_{60}F_{36}$ has allowed decreasing the isomer number to 63 [14], and 94 isomers have been selected in the case of $C_{60}F_{48}$ [13]. The justification of the assumption has been mainly based on the ^{19}F NMR spectra of $C_{60}F_{18}$ [18], $C_{60}F_{36}$ [19], and $C_{60}F_{48}$ [20, 21]. However, a thorough analysis of both ^{19}F NMR and two-dimensional correlation spectroscopy (2D COSY) spectra has shown that the structure assignment based on theoretical predictions is not absolutely secure, particularly for $C_{60}F_{36}$ and $C_{60}F_{48}$ species (see a detailed discussion in Secs. 5.4 and 5.5). Therefore, the problem of the assignment of the most stable isomers cannot be considered definitely solved.

An alternative approach to the problem can be suggested on the basis of the inherent regioselectivity of 60 pristine fullerene atoms. It is based on a partial radicalization of the C_{60} molecule caused by the appearance of effectively unpaired electrons (EUPEs) due to weakening of the interaction of its odd electrons [22–27]. These electrons, distributed over the cage atoms, enhance the atom chemical reactivity, providing a numerically definite atomic chemical susceptibility (ACS). Due to nonmonotonic EUPE distribution, the ACS mapping over cage atoms readily highlights target atoms that are characterized by the highest ACS. Thus, taking ACS as a quantitative pointer of the readiness of each atom to enter the chemical reaction allows making a definite choice of targets at each stage of the reaction and, consequently, performing a stepwise computational synthesis of fullerene derivatives of any composition. Exemplified by the first steps of the fullerene fluorination [25–27], the approach has turned out to be a proper tool for a stepwise synthesis of the halogenated $C_{60}(\mathrm{Hal})_{2k}$, hydrogenated $C_{60}H_{2k}$, aminated $C_{60}(\mathrm{Am})_m$ fullerene adducts in a predictable manner. In this paper, we present results related to the $C_{60}F_{2k}$ family. Hydrogenated and aminated families are discussed in [28, 29].

2. COMPUTATION METHODOLOGY

The traditional theory of chemical bonding involved conceptual and quantitative determination in terms of either bond [30] or Wiberg [31, 32] indices in the framework of the single-determinant close shell restricted Hartree–Fock (RHF) approximation. For odd-electron systems (the term indicates that the number of valence electrons of each fullerene atom is larger by one than the number of interatomic bonds formed by the atom), this corresponds to the limit case of strong coupling between the electrons. This requirement is met in the case of ethylene and benzene, where odd electrons are fully covalently coupled in the form of π electrons. However, even for naphthalene, not to mention higher acenes [33, 34], fullerenes [22–27], carbon nanotubes [33, 35, 36], and graphene [36], this is not the case due to the increased length of C–C bonds compared to those of the benzene molecule, which causes a noticeable weakening of the interaction between the electrons such that a part of odd electrons are excluded from the covalent coupling and become effectively unpaired.

Generalizing the approach to systems with weakly interacting electrons ultimately requires taking the electrons correlation into account and passing to computational schemes that involve the full configurational interaction. However, the traditional complete-active-space-self-consistent-field (CASSCF) methods that deal correctly with two electron systems of diradicals and some dinuclear magnetic complexes cannot handle systems with a large number of electrons due to a huge number of configurations generated in the active space of the system (for m singly occupied orbitals on each of the n identical centers, 2^{mn} Slater determinants should be formed by assigning spins up or down to each of the nm orbitals [37]). It has been assumed until recently that CASSCF-type approaches are non-feasible for many-odd-electron systems such as fullerenes, carbon nanotubes, and graphene. Hence, addressing single-determinant approaches appeared to be the only alternative.

The open-shell unrestricted broken spin-symmetry (UBS) approach suggested by Noodleman [38] is well elaborated for both wave-function and electron-density quantum-chemical methodologies, based on unrestricted single-determinant Hartree–Fock scheme [39] (UBS HF) and the Kohn–Sham single Slater determinant procedure of the density-functional theory (DFT), i. e. UBS DFT [40]. The main problem of the UBS approach concerns spin contamination of the calculation results. The interpretation of UBS results in view of their relevance to physical and chemical reality consists in mapping between the eigenvalues and eigenfunctions of the exact and model spin Hamiltonians. The implementation of the UBS HF approach, both *ab initio* and semiempirical, is standard and the desired mapping is quite straightforward. The recent first attempts of many-body configurational interaction calculations of polyacenes [34] and graphene [41] have provided a strong support of the UBS HF approach [36] and highlighted its high ability to quantitatively describe practically important consequences of the weak interaction between odd electrons of nanocarbons. A semiempirical UBS HF calculation scheme based on the AM1 approach was used in the current study; due to its high efficacy, massive calculations concerned with the isomerism of the $C_{60}F_{2k}$ family have been successfully performed.

3. SYNOPSIS OF THE VALUES UNDER CONSIDERATION

EUPEs provide a partial radicalization of the species and hence a considerable enhancement of its chemical reactivity. Because EUPEs are produced by spin-contaminated UBS solutions, they are directly related with the spin contamination

$$C = \langle \hat{S}^2 \rangle - S(S+1), \tag{1}$$

where $\langle \hat{S}^2 \rangle$ is the expectation value of the total spin angular momentum that follows from the UBS solution. Actually, as shown in [42], the total EUPEs number N_D is expressed as

$$N_D = 2\left[\langle \hat{S}^2 \rangle - \frac{(N^\alpha - N^\beta)^2}{4}\right], \tag{2}$$

where N^α and N^β are the respective numbers of electrons with spin α and β, and $N^\alpha - N^\beta$ determines the spin multiplicity. On the other side, the spin contamination produces an extra spin density (as is particularly evident for the singlet state), and hence N_D is expressed as the trace of the spin density [43],

$$N_D = \operatorname{tr} D(r|r'). \tag{3}$$

Therefore, to quantify N_D, either $\langle \hat{S}^2 \rangle$ or $\operatorname{tr} D(r|r')$ must be known.

For a single-Slater-determinant UBS HF function, the evaluation of both quantities is straightforward because the corresponding coordinate wave functions are subordinated to the definite permutation symmetry, and hence each spin value S corresponds to a definite expectation value of energy [44]. Therefore [45],

$$\langle S^2 \rangle = \frac{(N^\alpha - N^\beta)^2}{4} + \frac{N^\alpha + N^\beta}{2} - \sum_{i,j=1}^{NORBS} P_{ij}^\alpha P_{ij}^\beta, \tag{4}$$

where $P_{ij}^{\alpha,\beta}$ are the respective electron density matrix elements for spins α and β and $NORBS$ is the number of orbitals. Similarly, Eq. (3) has the form [25]

$$N_D = \sum_{i,j=1}^{NORBS} D_{ij}, \tag{5}$$

where D_{ij} are matrix elements of the spin density expressed as [25]

$$D = (P^\alpha - P^\beta)^2. \tag{6}$$

The last expression is related to the neglect-of-diatomic-differential-overlap (NDDO) approximation that underlies the AM1/PM3 semiempirical computational schemes. The summation in (5) ranges over all atomic orbitals.

The atomic origin of the UBS HF function produces another important relation concerning the partitioning of the N_D value over the system atoms,

$$N_D = \sum_{A}^{NAT} N_{DA}, \tag{7}$$

where NAT is the total number of atoms and [25]

$$N_{DA} = \sum_{i\in A} \sum_{B=1}^{NAT} \sum_{j\in B} D_{ij} \tag{8}$$

is attributed to the EUPEs number on atom A (the summation in (8) ranges over all atoms B except A). Because the EUPEs themselves are a "quality index" of the enhanced reactivity, the N_D and N_{DA} values just quantify the indices respectively representing the molecular and atomic chemical susceptibility (ACS). The correct determination of both values is well provided by the AM1/PM3 UBS HF solution [25] of the CLUSTER-Z1 software [46] used in the current study.

4. ALGORITHM OF COMPUTATIONAL SYNTHESIS OF FULLERENE DERIVATIVES

The analysis of the chemical activity of both carbonaceous and siliceous fullerenes presents the first practical implementation of the concepts described above [22–24]. From the standpoint of EUPEs, the C_{60} and C_{70} molecules are characterized by partial exclusion of odd electrons from the covalent bonding, which results in EUPEs constituting approximately a 10%-odd-electron fraction, while all odd electrons of the Si_{60} molecule are not paired, providing a 60-fold radicalization of the molecule. This finding highlights evident reasons for the failure to produce the species in practice. The ACS (N_{DA}) maps complete the structural description of the C_{60} and C_{70} molecules by their "chemical portraits" [25–27]. According to these papers, the C_{60} molecule consists of six identical naphthalene-core fragments forming a $6C_{10}$ configuration.

The chemical portrait of the C_{60} molecule is shown in Fig. 1*a* and *b*, and the ACS map of the molecule atoms belonging to groups 1–5 is presented in Fig. 1*c*. According to the figure, the initial step of any additional chemical reaction involves atoms of the highest ACS of group 1. There are 12 identical atoms that form 6 short C–C bonds belonging to 6 identical naphthalene-core fragments. We may choose any of the pairs to start the reaction of attaching any R addend to the fullerene cage, including fluorine atoms and/or molecules. When the first adduct $C_{60}R_1$ is formed, the reaction should proceed around the cage atoms with the largest N_{DA} values resulting in the formation of adduct $C_{60}R_2$. A new ACS map reveals the sites for the next addition step, and so on. The reaction is terminated when all the N_{DA} values are fully exhausted. Following this methodology, a complete list of fluorinated fullerenes $C_{60}F_{2k}$ has been synthesized.

5. RESULTS AND DISCUSSION

5.1. Start of the C_{60} fluorination

When starting the fluorination of C_{60}, one fluorine molecule is placed in the vicinity of the selected atoms of group 1 (31 and 32 in the current case) (Fig. 2*a*) and a full optimization of the complex geometry in the singlet state is performed. It turns out that the fluorine molecule is willingly attached to the cage, but two adducts are possible depending on the fluorine molecule orientation with respect to the chosen C–C bond. If the molecule axis is parallel to the bond, adduct $C_{60}F_2$ (adduct I, Fig. 2*b*) is formed. If the molecule axis is even slightly inclined toward the bond, a complex $C_{60}F_1 + F$ (adduct II + F, Fig. 2*c*) is obtained.

Figure 3 presents the ACS maps of the pristine C_{60} cage (gray) and of the cage after formation of adducts I and II (black) following the atom numeration in the output file. The crosses mark the initial target atoms 31 and 32. As can be seen from the figure, attaching either one or two fluorine atoms changes the initial map considerably and differently in both cases. When two atoms are attached to the cage, the N_{DA} values become zero for target atoms 31 and 32 and star-marked atoms 18, 20, 38, and 55 become the most active (Fig. 3*a*). When one atom is attached, the remaining target atom 31, which is adjacent to the first target atom 32, dominates on the adduct ACS map (Fig. 3*b*). The picture clearly evidences the readiness of the C_{60} cage to complete the reaction by adding a further fluorine atom to atom 31. Following this indication, and keeping configuration of the II + F complex, we add the second fluorine molecule as shown in Fig. 2*d*. In due course of the structure optimization, a new adduct $C_{60}F_2 + 2F$ (III + 2F, Fig. 2*e*) is formed. Geometry and electronic properties of adduct III are fully identical to those of adduct I, which is also confirmed by a complete identity of their N_{DA} maps. Therefore, in-

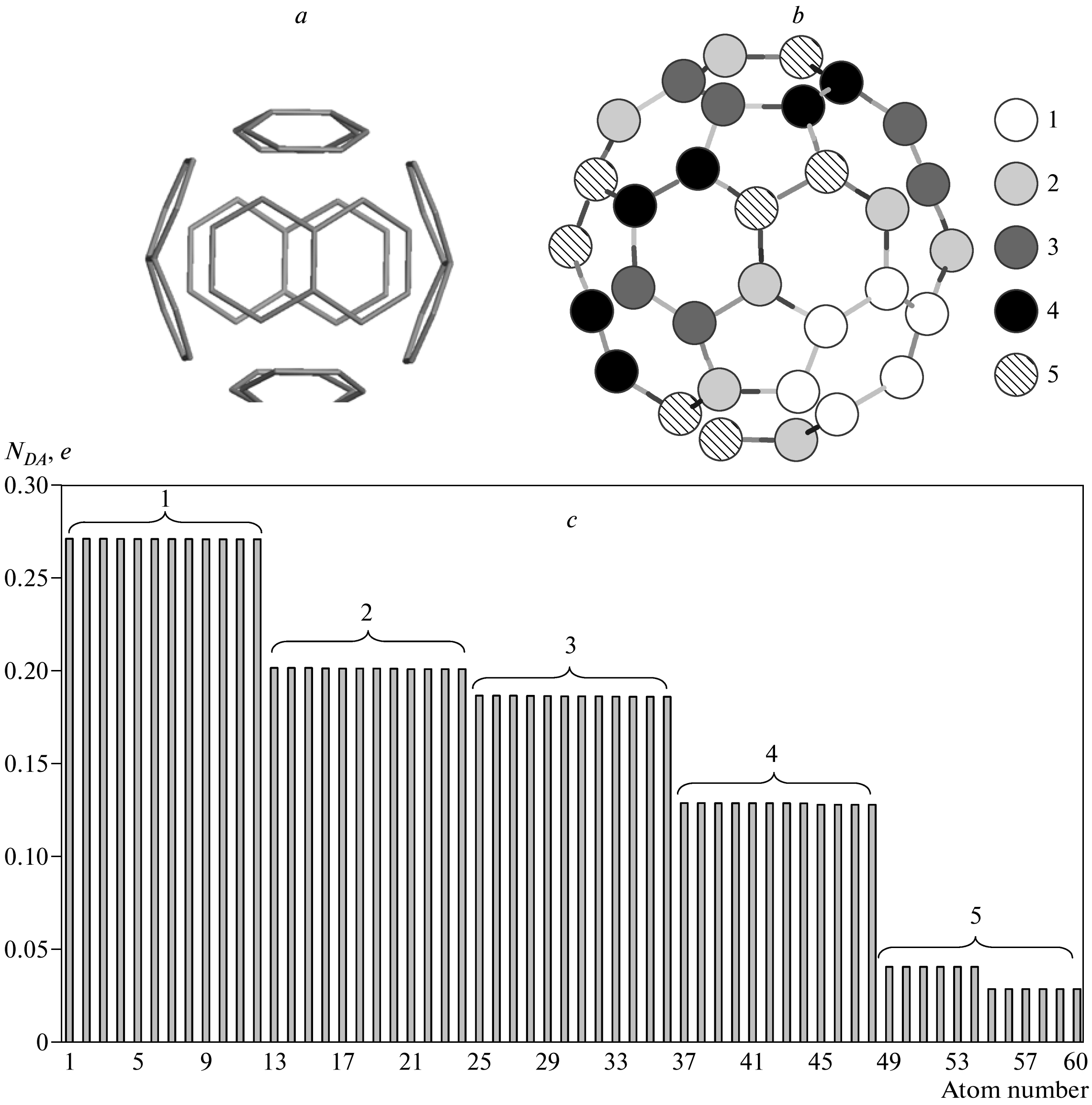

Fig. 1. Chemical portrait of C_{60} [26] the $6\mathrm{C}_{10}$ composition (*a*); different colors mark atoms with different ACS (*b*). Figures point to different atom groups, and ACS map over atoms of C_{60}; N_{DA} data are aligned from the largest value down (*c*)

dependently of whether the one-stage (see Fig. 2*b*) or two-stage (Fig. 2*e*) process of the F_2 attachment to the fullerene cage occurs, the same final adduct $\mathrm{C}_{60}\mathrm{F}_2$ is formed. Obviously, the two-stage reaction should prevail in practice. It is radical by nature and follows a qualitative scheme suggested in [47].

The next step of the reaction is governed by the predominance of atoms 18, 20, 38, and 55 on the ACS map of $\mathrm{C}_{60}\mathrm{F}_2$ (see Fig. 3*a*) over other atoms. The above atoms form two identical pairs of short C–C bonds located in the equatorial plane with respect to the first two target atoms (see white atoms in Fig. 4*a*). One of these pairs is taken as targeting and the procedure of attaching F_2 to the pair atoms repeats the one described above. Consequently, a $\mathrm{C}_{60}\mathrm{F}_4$ molecule is formed (Fig. 4*b*). The ACS map is calculated for the product to select target atoms for the next attaching. As can be seen from Fig. 4, a subsequent F_2 addition is not contiguous (Fig. 4*c*) as was suggested in [4, 6].

From the computational standpoint, the result of one-atom addition at each stage of the two-stage process of the F_2 addition is independent of precisely which, molecular or atomic, addend attacks the cage. That is why a subsequent addition of fluorine atoms

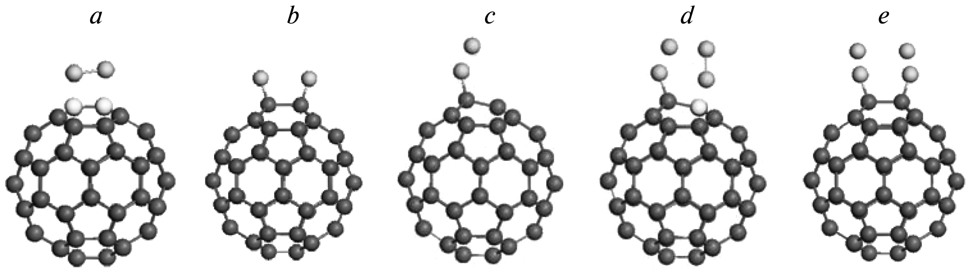

Fig. 2. Attachment of one (a–c) and two (d,e) fluorine molecules to the C_{60} cage: a — the starting geometry; target atoms of the C_{60} cage are white; b — adduct I $C_{60}F_2$; c — adduct II $C_{60}F_1$ and a free fluorine atom F; the composition corresponds to the starting geometry in a; starting configuration (the target atom of the C_{60} cage is white) (d) and final adduct III (e) of the reaction ($C_{60}F_1 + F + F$)

one-by-one is considered in what follows as a series of successive steps consisting of two stages, which involves calculations of two adducts related to the two reactions,

$$C_{60}F_{2k} + F = C_{60}F_{2k+1}$$

and

$$C_{60}F_{2k+1} + F = C_{60}F_{2(k+1)},$$

$k = 1, 2, \ldots, 30$. Each step is controlled by the fullerene cage ACS map of the preceding adducts, namely, $C_{60}F_{2k}$ and $C_{60}F_{2k+1}$. Actually, when the difference between the high-rank N_{DA} values is not significant, every step is additionally complicated by expanding calculations over a restricted set of isomers that are selected by a set of high-rank values on the ACS map. A final choice of the most stable species is thus subordinated to the preference of the structure with the least total energy.

5.2. $C_{60}F_2$–$C_{60}F_8$ adducts

We consider the synthesis of fluorinated adducts in the working regime exemplifying the procedure for $C_{60}F_2$–$C_{60}F_8$ adducts. Chart 1 presents high-rank N_{DA} values of the species from C_{60} to $C_{60}F_8$. The N_{DA} data are ordered from top down and only a small part of high-rank data is shown. Fluorinated adducts are marked FN, where N marks the number of added fluorine atoms.

Cage atom 32 was chosen as the first one to be attacked by fluorine. Atom 31 heads the list of the N_{DA} data of adduct F1 and obviously points to the place of the next attack. The head of the N_{DA} list of F_2 involves two pairs of one-bond-connected atoms 38&55 and 20&18 (they are shown in Fig. 4a). The pairs are fully equivalent and, as shown by calculations, the series of adducts starting from each of them are also equivalent. We proceed with atom 38 to form F3, whose N_{DA} list immediately highlights the pairing atom 55. The N_{DA} list of F4 is opened by one-bond-connected atoms 42&48 and includes atom 22, whose pair atom is shifted into the depth of the list. Continuing addition by attacking atom 42, we obtain F5 with atom 48 having the highest N_{DA}. The N_{DA} list of F6 is typical for the majority of successive addition events and is headed by two (sometimes, three) atoms with comparable N_{DA} values, while the corresponding one-bond-connected atoms are shifted into the depth of list. Two such pairs of F6 are shown differently in Chart 1. This is a typical case where a study of a few isomers is needed. The first isomer F7-1 corresponds to attacking atom 60 and highlights atom 59 for the next attack. The second isomer F7-2 starts on atom 58 and exhibits its pairing atom 57. Two F_8 adducts followed from these two F7 isomers differ by the total energy, respectively given by 517.162 and 517.216 kcal/mol for isomers F8-1 and F8-2. In spite of a seemingly small difference in the energy, isomer F8-1 is favored quite reliable. Checking series from F8-1 and F8-2 isomers showed that all the subsequent species have a much higher total energy in the second case. Atomic views of the F2k species for k = 1, 2, 3, 4 are shown among the others in Fig. 5. As can be seen from the figure, neither F4 nor F6 and F8 follow the contiguous scheme of the addition suggested in [4]. Not the hypothetical growth of the aromaticity of adjacent bonds but the redistribution of the EUPE density over the cage atoms is the governing factor of the reaction pathway.

The total energy of adducts and their main geometric parameters are presented in Table 1. This concerns C*–F and C*–C* bond lengths, where C* denotes cage atoms bound to a fluorine one. Changing the total energy in due course of fluorination is shown in Fig. 6 as

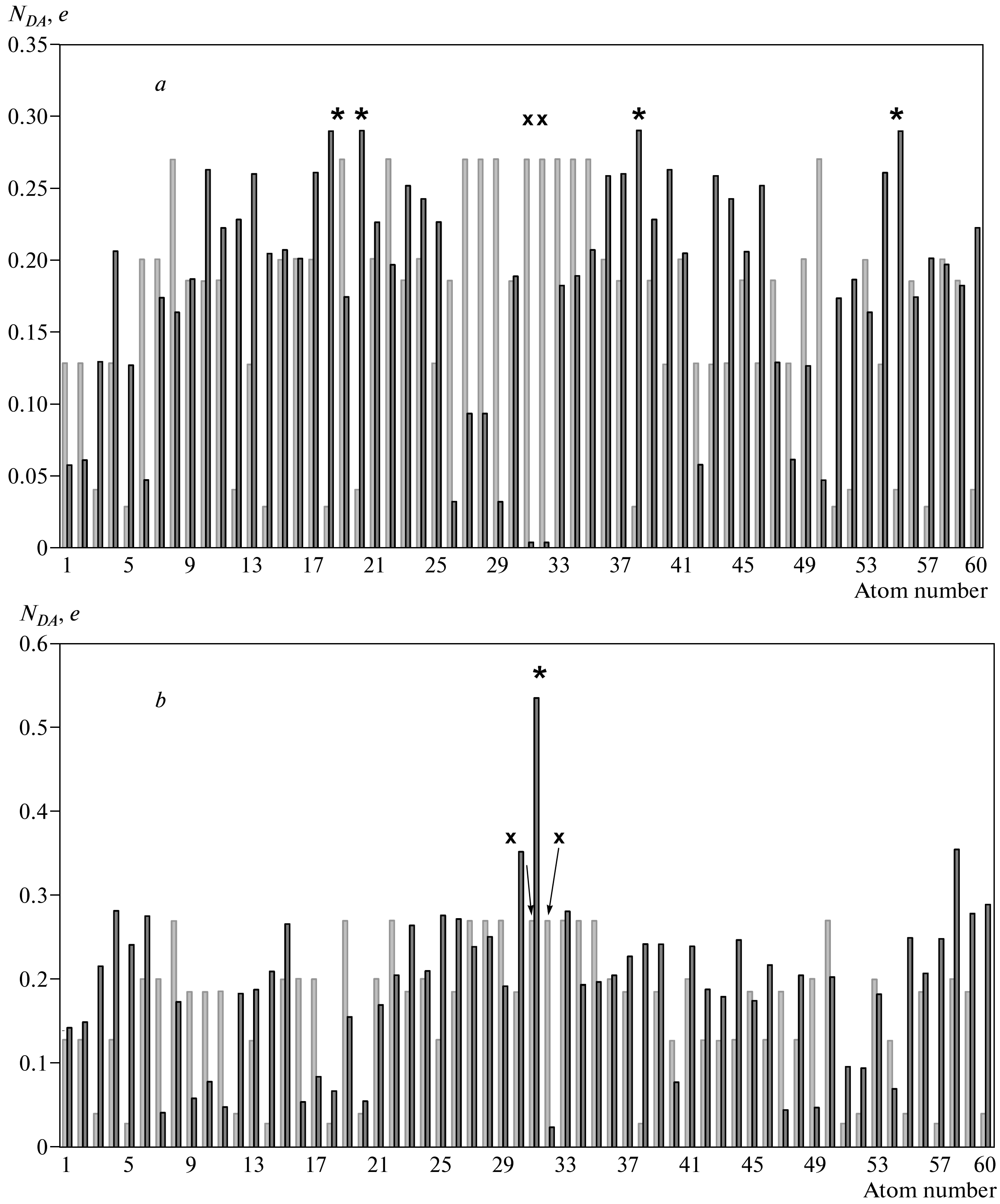

Fig. 3. ACS map of the C_{60} cage of the adducts $C_{60}F_2$ (a) and $C_{60}F_1$ (b). Gray bars present the map of the pristine C_{60} molecule

a function of the coupling energy E_{cpl} needed for the addition of every next pair of fluorine atoms from the pair number k. Assuming that the reaction occurs in the gaseous fluorine, we express the energy as

$$E_{cpl} = \Delta H_{2k} - \Delta H_{2(k-1)} - \Delta H_{F_2}, \qquad (9)$$

where ΔH_{2k} and $\Delta H_{2(k-1)}$ are heats of formation of F2k and F2(k−1) products, and ΔH_{F_2} is the heat of formation of the fluorine molecule, equal

Chart 1. F1 to F8 fluorination. Figures in brackets show the number of the C_{60} cage atom to which the current fluorine atom is attached

F0–C60		F1 (32)		F2 (31)		F3 (38)		F4 (55)	
Atom number	N_{DA}	Atom number	N_{DA}	Atom number	N_{DA}	Atom number	N_{DA}	Atom number	N_{DA}
32	**0.27072**	**31**	**0.53894**	**38**	**0.29094**	**55**	**0.51918**	**42**	**0.30143**
31	**0.27077**	35	0.35590	*20*	*0.29086*	40	0.33620	22	0.30002
		33	0.35406	**55**	**0.29049**	4	0.31575	**48**	**0.30000**
		39	0.29065	*18*	*0.29041*	20	0.29535	2	0.29971
		30	0.28358	10	0.26369	18	0.29026	1	0.28812
		10	0.28304	40	0.26368	36	0.28537	35	0.29782
		F5 (42)		F6 (48)		F7-1 (60)		F8-1 (59)	
		Atom number	N_{DA}	Atom number	N_{DA}	Atom number	N_{DA}	Atom number	N_{DA}
		48	**0.52989**	**60**	**0.34210**	**59**	**0.51853**	**22**	**0.34686**
		39	0.35424	*58*	*0.32535*	57	0.37960	*24*	*0.32989*
		22	0.34896	22	0.28518	39	0.37006	54	0.29221
		36	0.34284	1	0.28104	46	0.36312	27	0.28239
		35	0.34226	39	0.27708	60	0.34821	11	0.28026
		49	0.34028	44	0.27568	22	0.34667	36	0.27552
				35	0.27411			35	0.27273
				59	**0.26879**			*23*	*0.27116*
				15	0.26840			28	0.27074
				2	0.26778			**33**	**0.26836**
				26	0.26445			25	0.26625
				12	0.26395			6	0.26346
				57	*0.26360*			44	0.26253
				5	0.25955			53	0.26195

to −22.485 kcal/mol. The data lay within the [−91; −83] kcal/mol interval, demonstrating a tight binding of fluorine with the fullerene cage. The corresponding best values for F2 and F4 obtained in [10] in the close-shell RHF AM1 approximation and corrected by ΔH_{F_2} are practically constant and amount to -63.5 ± 0.2 kcal/mol. The data increase by about 1.5 times when passing from the RHF to the UHF approximation. Close-shell B3LYP/4_31G calculations in the B3LYP/STO-3G geometry result in the respective appropriately ΔH_{F_2}-corrected values −92.4 and −101.7 kcal/mol for F2 and F4 species [5], which are close to the UBS HF results.

As can be seen from Table 1, the total energy markedly decreases when fluorination proceeds, which favors polyaddition. This actually occurs experimen-

Table 1. Geometric parameters and total energy of fluorinated fullerenes $C_{60}F_{2k}$

	F1	F2	F3	F4	F5	F6
$R(C^*–F)$, Å[a]	1.378	1.382	1.382, 1.378	1.382	1.382, 1377	1.382
$R(C^*–C^*)$, Å[b]	1.52	1.61	1.52	1.62, 1.61	1.52,	1.61
ΔH, kcal/mol[c]	903.60	843.58	795.50	729.99	677.70	622.58
Symmetry		C_{2v}		C_s		C_1
	F7	F8	F10	F12	F14	F16
$R(C^*–F)$, Å[a]	1.383–1.381	1.384–1.381	1.383–1.381	1.383–1.381	1.387–1.380	1.385–1.378
$R(C^*–C^*)$, Å[b]	1.52	1.61–1.60	1.61–1.60	1.61–1.58	1.60–1.58	1.60–1.57
ΔH, kcal/mol[c]	570.35	517.16	414.70	305.92	195.77	86.80
Symmetry		C_1	C_1	C_1	C_1	C_s
	F18	F20	F22	F24	F26	F28
$R(C^*–F)$, Å[a]	1.384–1.377	1.385–1.376	1.384–1.375	1.385–1.375	1.385–1.374	1.386–1.376
$R(C^*–C^*)$, Å[b]	1.58–1.57	1.59–1.57	1.59–1.57	1.59–1.57	1.59–1.57	1.58–1.57
ΔH, kcal/mol[c]	−24.54	−132.87	−248.07	−355.61	−459.33	−552.60
Symmetry	C_{3v}	C_1	C_1	C_1	C_s	C_1
	F30	F32	F34	F36	F38	F40
$R(C^*–F)$, Å[a]	1.385–1.374	1.393–1.373	1.393–1.376	1.402–1.375	1.402–1.375	1.402–1.376
$R(C^*–C^*)$, Å[b]	1.59–1.57	1.59–1.57	1.59–1.57	1.59–1.57	1.59–1.57	1.59–1.57
ΔH, kcal/mol[c]	−642.47	−738.80	−822.14	−914.95	−905.77	−1069.62
Symmetry	C_1	C_1	C_1	C_1	C_1	C_1
	F42	F44	F46	F48	F50	F52
$R(C^*–F)$, Å[a]	1.402–1.381	1.402–1.381	1.402–1.383	1.408–1.387	1.408–1.387	1.410–1.387
$R(C^*–C^*)$, Å[b]	1.59–1.57	1.59–1.57	1.59–1.57	1.59–1.57	1.59–1.57	1.59–1.57
ΔH, kcal/mol[c]	−1120.36	−1184.68	−1237.16	−1293.30	−1338.08	−1356.10
Symmetry	C_1	C_1	C_1	C_1	C_1	C_s
	F54	F56	F60			
$R(C^*–F)$, Å[a]	1.412–1.387	1.412–1.385	1.412–1.357			
$R(C^*–C^*)$, Å[b]	1.59–1.57	1.59–1.57	1.585–1.565			
ΔH, kcal/mol[c]	−1371.49	−1387.42	−1410.63			
Symmetry	C_s	C_s	I_h			

[a] C^* marks a cage atom to which fluorine is added.

[b] $C^*–C^*$ marks a pristine short bond of the cage to which a pair of fluorine atoms is added.

[c] ΔH is the heat of formation determined as $\Delta H = E_{tot} - \sum_A (E^A_{elec} + E^A_{heat})$, where $E_{tot} = E_{elec} + E_{nucl}$, while E_{elec} and E_{nucl} are the elctron and core energies; E^A_{elec} and E^A_{heat} are the electron energy and the heat of formation of an isolated atom A, respectively.

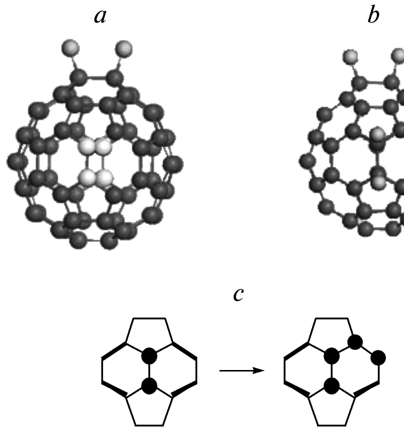

Fig. 4. Attachment of one fluorine molecule to the $C_{60}F_2$ cage: *a* — the starting geometry; target atoms of the C_{60} core are white; *b* — adduct $C_{60}F_4$; *c* — a scheme of contiguous F_2 addition [4]

tally, and $C_{60}F_{18}$, $C_{60}F_{36}$, and $C_{60}F_{48}$ are usually the main products obtained [6]. As shown by groups of Taylor and Boltalina (see reviews [2,4]), the fluorination yield greatly depends on the reaction conditions. In fluorination by a fluorine gas, the electron ionization mass spectrum showed a continuous spectrum of derivatives from $C_{60}F_2$ to $C_{60}F_{42}$. However, it was unclear whether the lower fluorinated species were compounds or merely fragmentation ions. Only after particular measures were taken, the authors succeeded in separating lower fluorinated species $C_{60}F_2$, $C_{60}F_4$, $C_{60}F_6$, and $C_{60}F_8$ [48,49], confirming the stability of adducts.

The top panel in Fig. 6 shows the EUPEs total number as a function of the number of fluorinated pairs added to the fullerene cage. The value gradually decreases when fluorination proceeds, and hence the molecular chemical susceptibility N_D logically behaves as a "pool of chemical reactivity" that is being worked out in the course of the reaction. At the very beginning at low k, N_D slightly increases due to an increase in the number of elongated unfluorinated C–C bonds caused by the sp^2–sp^3 cage structure reconstruction under fluorination.

5.3. $C_{60}F_{10}$–$C_{60}F_{18}$ adducts

A detailed procedure of computational fluorination of the C_{60} cage discussed above is retained through the full cycle of the $C_{60}F_2$ to $C_{60}F_{60}$ fluorination. A concise synopsis related to the formation of products from $C_{60}F_{10}$ to $C_{60}F_{18}$ that required a study of 11 isomers is presented in Chart 2. The content of each cell involves the isomer name and the cage atom numbers, which were taken from the high-rank part of the N_{DA} list of the preceding isomer and addition to which provided the current isomer formation, as well as the isomer total energy in kcal/mol. Isomers with the least total energy are shown in boldface. When reading the chart, the following picture is developed. Starting with isomer F8-1 and looking at the N_{DA} list in Chart 1, we can obtain two isomers F10 by adding a pair of fluorine atoms to either atoms 22 and 33 (F10-1) or atoms 24 and 23 (F10-2). The total energies of the two isomers are 414.700 and 415.812 kcal/mol. The energy difference favors the first one, which we place at the head of the $C_{60}F_{10}$–$C_{60}F_{18}$ series in Chart 2. The high-rank part of the list of F10-1 involves three pairs that originate three F12 isomers shown in Chart 2. Isomer F12-2 has the least energy and a fluorine atom addition to its high-rank atoms produces two F14 isomers. Choosing the F14-1 isomer, we proceed with two F16 isomers, among which F16-2 is more favorable energetically. Adding fluorine atoms to atoms 23 and 24 of F16-2, we obtain isomer F18-1. Shown for comparison in Chart 2 is the case where adduct F18 is produced from isomer F16-1. As can be seen from the chart, thus formed F18-2 and F18-3 adducts have much higher energy and are energetically nonprofitable with respect to adduct F18-1.

Equilibrated structures of adducts from the $C_{60}F_{10}$–$C_{60}F_{18}$ series that correspond to those of the least total energy are shown above in Fig. 5. Drawn in the same projection, the pictures allow vividly exhibiting a consequent deformation of the fullerene cage caused by fluorination until F18 is formed. The last row of pictures in Fig. 5 presents F18 in different projections to highlight its crown-like structure of the C_{3v} symmetry well known experimentally [50–52]. The total energy and geometric parameters of adducts are given in Table 1. Data plotting in Fig. 6 shows that both N_D and the coupling energy do not differ much within the series and retain close to the highest values just revealing the high chemical reactivity of individual adducts and a strong tendency to further fluorination.

5.4. $C_{60}F_{20}$–$C_{60}F_{36}$ adducts

Continuing the computational procedure, a series of $C_{60}F_{20}$–$C_{60}F_{36}$ adducts was produced. About 20 isomers were considered in order to choose the most stable isomers. Such selected isomers are shown in Fig. 7, and their total energy and geometric parameters are given

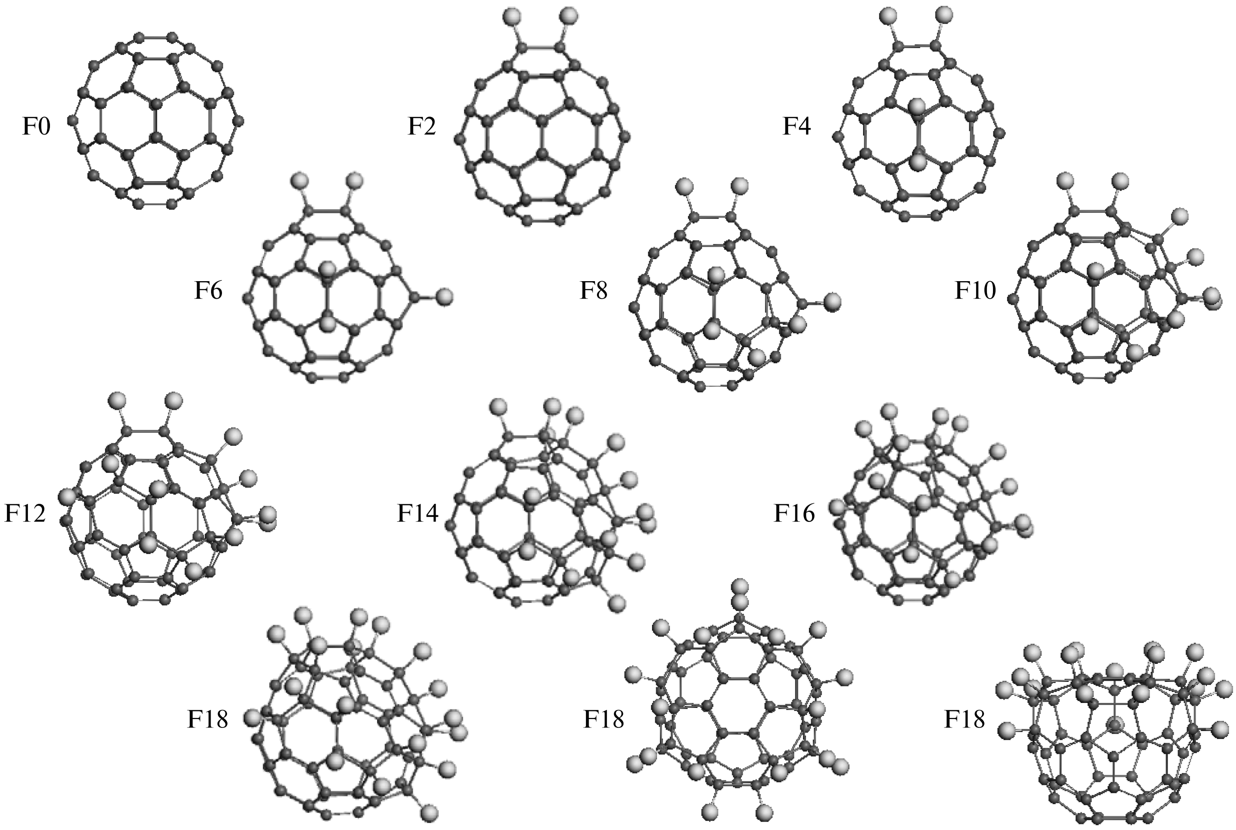

Fig. 5. Equilibrium structures of $C_{60}F_0$ to $C_{60}F_{18}$ fluorinated fullerenes

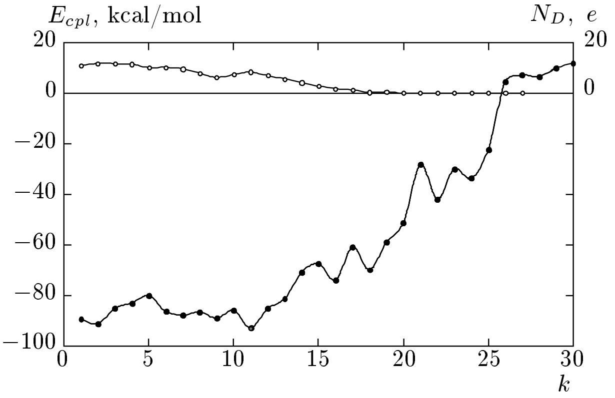

Fig. 6. Evolution of the N_D value and the coupling energy E_{cpl} with the number k of fluorine atom pairs

in Table 1. In contrast to the previous series, the current one does not end by a high-symmetry adduct. The obtained F36 adduct has no symmetry at all.

Fluoride $C_{60}F_{36}$ is one of the most studied among other fluorinated fullerenes. However, since the first recording of the substance [53] (and until the last one [54]), there has not been clear vision of the composition and symmetry of the species. A strong temptation to see a direct connection between F18 and F36 [6] motivated searching for C_3-based structures of F36 both computationally [14–17] and experimentally [52, 54–57]. However, all experimental findings turned out to have a complicated structure and cannot be interpreted from the high-symmetry standpoint. This led to the conclusion about a complicated isomer composition of the produced material, involving isomers of the C_3, C_1, and T symmetry. Another view on the problem might be based on the computed F36. This concerns interpreting the experimental findings not from a rigid "yes/no" symmetry standpoint (C_1 or other symmetry) but in terms of continuos symmetry [58, 59]. We cannot exclude that fitting experimental and computational data could then be quite satisfactory, as this is in the case with C_{60}, whose exact symmetry is C_i, but a continuous symmetry is I_h [26, 60].

As can be seen from Fig. 6, fluorination of F20 to F36 covers the main step at which the pool of the cage

Chart 2. Scheme of F8–F18 fluorination

<table>
<tr><td colspan="6">**F8-1**
60&57
517.162</td></tr>
<tr><td colspan="6">**F10-1**
22&33
414.700</td></tr>
<tr><td>F12-1
54&40
310.952</td><td colspan="4">**F12-2**
52&51
305.920</td><td>F12-3
53&56
311.329</td></tr>
<tr><td></td><td colspan="3">**F14-1**
58&59
198.577</td><td>F14-2
53&56
203.669</td><td></td></tr>
<tr><td></td><td colspan="2">F16-1
53&56
87.656</td><td>**F16-2**
40&54
86.799</td><td colspan="2"></td></tr>
<tr><td></td><td>F18-2
24&23
−18.287</td><td>F18-3
16&11
−8.705</td><td>**F18-1**
24&23
−24.538</td><td colspan="2"></td></tr>
</table>

chemical reactivity is being worked out. The remaining N_D values become small. Simultaneously, the coupling energy considerably decreases in absolute value. Both factors evidently point to weakening the reaction ability, which evidences the reaction termination in a few steps.

5.5. $C_{60}F_{38}$–$C_{60}F_{48}$ adducts

Due to the smallness of the N_D value, the next steps of the addition reaction require more attention and a thorough investigation of a number of isomers at each step. Nevertheless, with a few roots of the reaction continuation attempted, the same set of energetically stable isomers has been obtained. The species are presented in Fig. 8. Their total energy and geometric parameters are given in Table 1. As can be seen from Fig. 8, the structure of adducts becomes visually more and more symmetric as the fluorination proceeds. However, the point symmetry of F48 is C_1.

Analyzing Fig. 6 at this stage of the reaction, one should conclude that experimental realization of high-fluorinated C_{60} is approaching the end because 1) the chemical reactivity pool is worked out and 2) the coupling energy actively decreases, approaching zero. Therefore, F44–F50 must be the final species in the row of fluorinated C_{60} because the coupling energy of F52 and higher species becomes positive. One of the first report on producing F48 [61] states that the substance can be obtained only in the course of long-time fluorination and that depending on the temperature either F46 or F48 species can be obtained. Both species are due to the polyaddition realization inherent to the fluorination process. Just stopping the reaction afterwards allows accumulating the species in a considerable amount. This makes the production of F48 more favorable than the production of either F18 or F36 in spite of much worse conditions for the reaction occurrence as regards N_D values and the coupling energy. As for higher fluorinated fullerenes, no indication of their observation is known [6] besides F60 that was supposedly observed as trace amounts in an ^{19}F NMR study [6].

Fluoride F48 is the main target of the stage on which considerable effort was concentrated. The first ^{19}F NMR analysis of the species showed [61] that when the NMR spectrum of F46 is very complicated, that of F48 demonstrates clear patterns characteristic of high symmetry. It was suggested that two chiral isomers of the D_3 symmetry formed the studied sample. All further investigations were aimed at proving the high symmetry of the species, both computationally [13, 16] and experimentally [57, 62–64]. In spite of many efforts

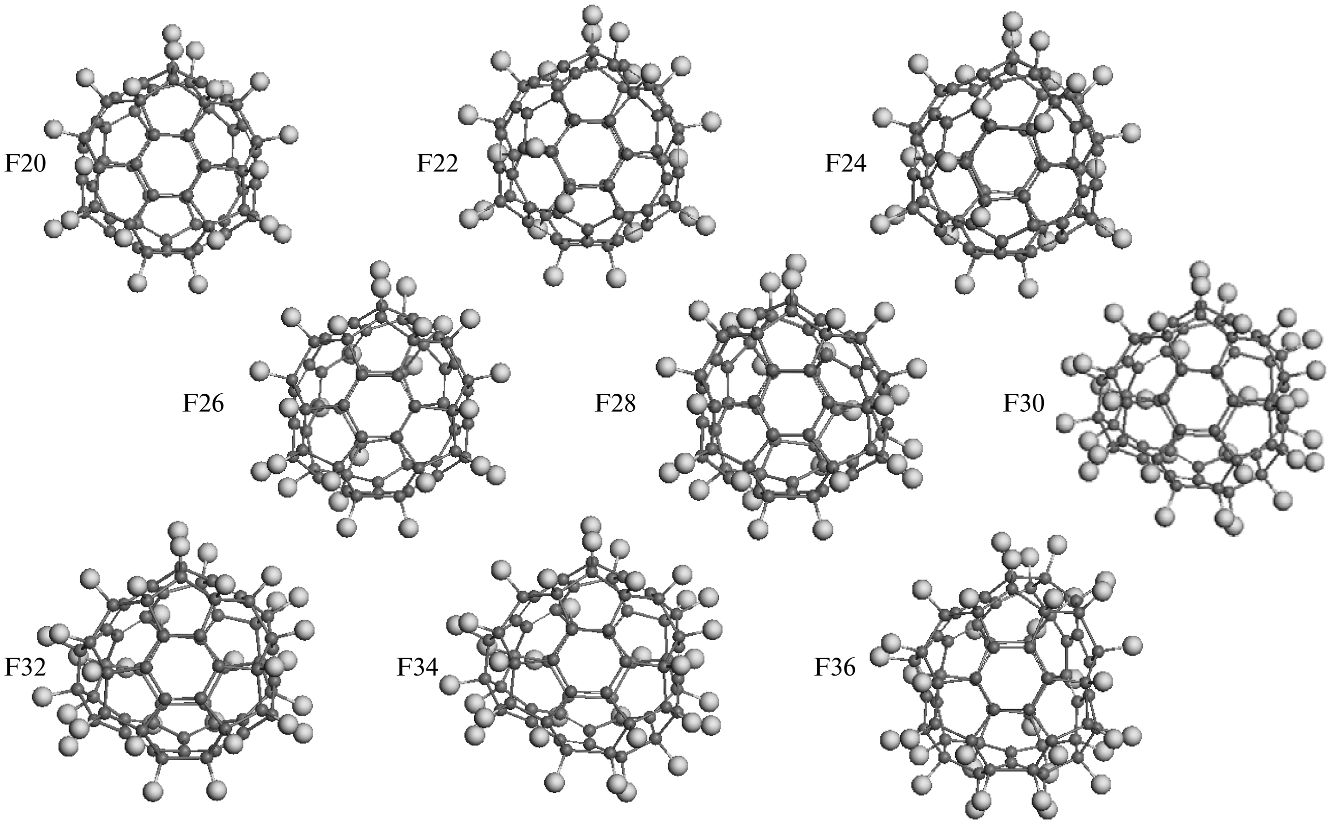

Fig. 7. Equilibrium structures of $C_{60}F_{20}$ to $C_{60}F_{36}$ fluorinated fullerenes

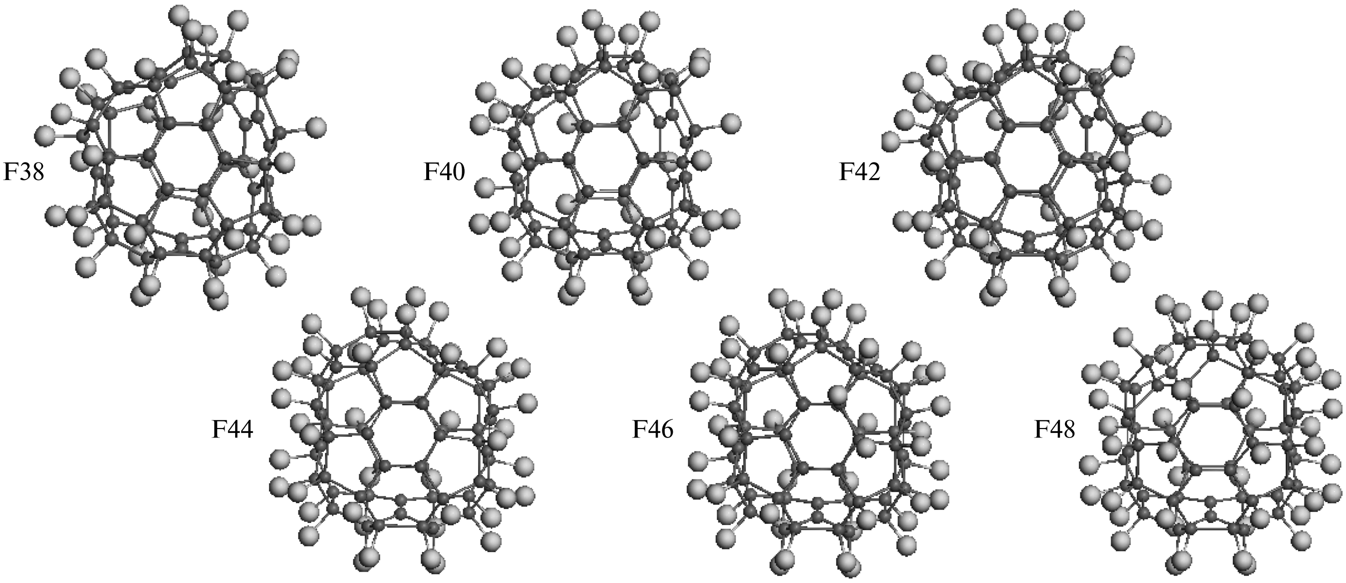

Fig. 8. Equilibrium structures of $C_{60}F_{38}$ to $C_{60}F_{48}$ fluorinated fullerenes

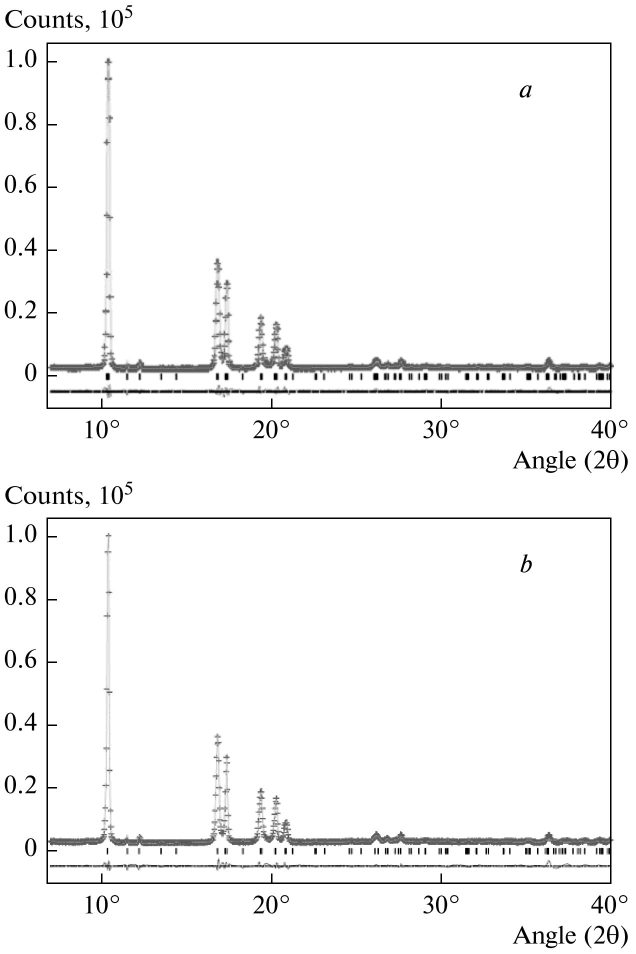

Fig. 9. Plots of the best Rietveld refinements associated with D_3 [64] (a) and C_1 [65] (b) molecular models of $C_{60}F_{48}$. Courtesy by Dr. R. Papoular, Leon Brillouin Laboratory, CEN-Saclay

undertaken to clarify the symmetry problem, there are still features that do not fit the high-symmetry suggestion. Those are extra dots on the $2D$ COSY ^{19}F NMR diagram [61], and the insufficient accuracy of gas electron diffraction due to a large number of parameters used in interpreting the data obtained [63]. This can also be addressed to high-resolution X-ray powder diffraction [64], and hence only a relative conclusion could be made that, e. g., the D_3 symmetry of the molecule fits experimental data under applied conditions better than the S_6 or T_d symmetry. Under these conditions, it was interesting how precisely may the experimental data fit the structure shown in Fig. 8. R. Papoular from the Leon Brillouin Laboratory, CEN–Saclay, agreed to perform Rietveld refining of his high-resolution X-ray powder diffraction structure data for $C_{60}F_{48}$ powder by using the F48 molecular structure following from the current study [65]. Figure 9 presents the refining results for the molecule in comparison with those obtained for D_3-symmetric species. The latter was accepted as the best fit in comparing molecular structures of D_3, S_6, and T_d symmetries [64]. As can be seen from the figure, the fit for the C_1 molecule is visually not only worse than that of the D_3 symmetry but even better in the region of the first most intensive peak. Table 2 summaries the results of numerical comparison of the two Rietveld refinements added by the data for an S_6 molecule. It can be concluded that the C_1 molecule refinement is between D_3 and S_6 ones, that is why we were led to the conclusion that it was either D_3 or S_6, when we did not know the molecule symmetry. At any rate, the molecule had to be attributed to a high symmetry, not to C_1 that formally follows from the molecule structure.

Table 2. $C_{60}F_{48}$ Rietveld refinement [64, 65]

Quality factors	Symmetry		
	D_3	C_1	S_6
χ^2	0.1481	0.1708	0.1870
wRp	0.0356	0.0382	0.0399
Rp	0.0383	0.0435	0.0438
R (F2)	0.0758	0.0766	0.0906
Durbin–Watson d-statistics	0.6190	0.4810	0.5000

As regards the discussed X-ray diffraction case, the Rietveld refinement started from the modeling of crystal packing. This procedure involves a large set of approximations (the 6-exp-1 intermolecular potential, a particular algorithm of the Coulomb energy calculation, and so on), which make the refining procedure dependent on numerous parameters. Not all of them are physically real. For example, in calculating the Coulomb energy within the bond-center charge model, the respective charges $-0.086e$ and $-0.380e$ on C and F atoms of each C–F bond and the charge $0.466e$ on the charge center in the bond middle were assumed [64], while the unfluorinated carbons had no charge. This assumption drastically contradicts the real picture of charge distribution over the molecule atoms, which is shown in Fig. 10. The F48 fluoride is presented in the figure by D_3 (the curve with open circles) and C_1 (the histogram) molecules. The structure of the former was taken as suggested in [65]. Just this D_3 molecule was used for the Rietveld refinement in [64]. As follows

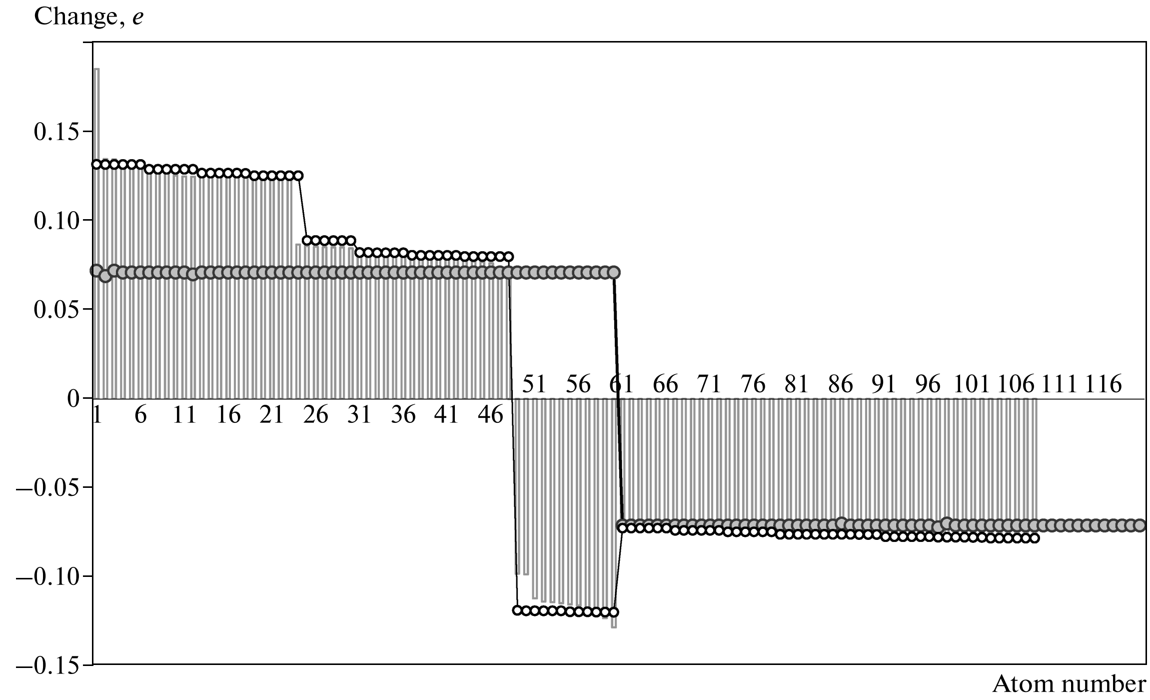

Fig. 10. Charge distribution over atoms of $C_{60}F_{48}$ (the histogram is the C_1 molecule and the curve with empty dots is the D_3 molecule) and $C_{60}F_{60}$ (curve with filled dotes) species

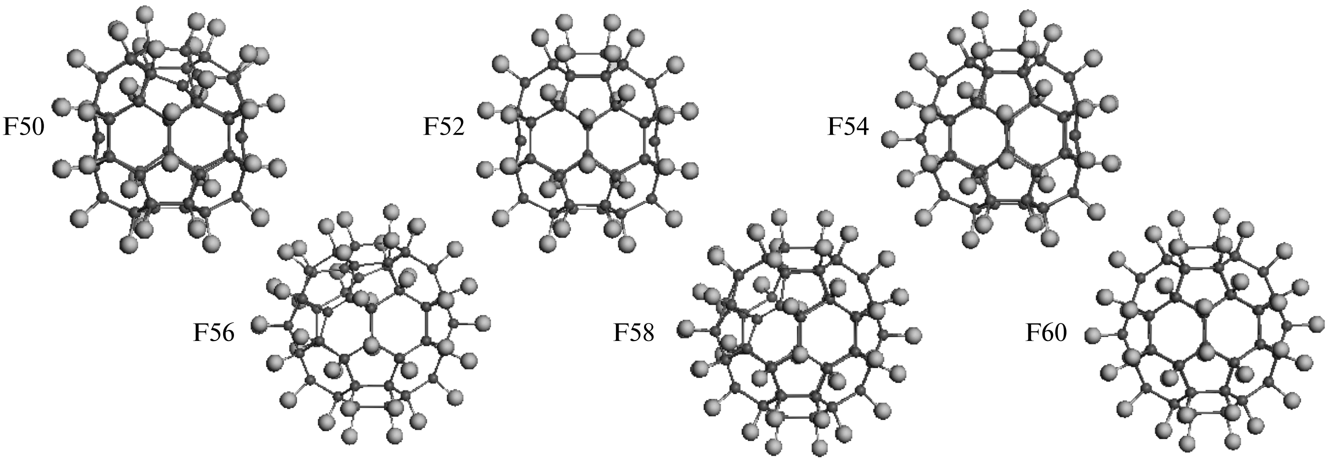

Fig. 11. Equilibrium structures of $C_{60}F_{50}$ to $C_{60}F_{60}$ fluorinated fullerenes

from the figure, the general pattern of the charge distribution is well similar for both molecules. The difference between the two plots just reflects the difference in the molecule symmetry. In both cases, fluorinated carbon atoms form three main groups with charges of the first group within $0.135e$–$0.123e$ (C_1) (a spike at $0.185e$ is a direct evidence of low symmetry) and $0.132e$–$0.125e$ (D_3) intervals; of the second group, within $0.087e$–$0.073e$ (C_1) and $0.089e$–$0.080e$ (D_3) intervals; and of the third group, from $-0.098e$ to $-0.128e$ (C_1) and at $-0.119e$ (D_3). The first group involves atoms one of whose neighbors is not fluorinated. All atoms of the second group are fluorinated and are joined to fluorinated atoms. Atoms of the third group are unfluorinated. Fluorine atoms have charge within the intervals from $-0.072e$ to $-0.080e$ (C_1) and from

$-0.072e$ to $-0.078e$ (D_3). When fluorination is fully completed in $C_{60}F_{60}$, the charges of both carbon and fluorine atoms are practically constant, equal in absolute value ($0.071e$ and $-0.071e$) and opposite in sign. As can be seen from Fig. 10, the real charge distribution has nothing in common with the assumptions made in [64]. And who knows, if these charges were taken into account, not a D_3 but a C_1 molecule would have been the best fit for the Rietveld refinement. At any rate, the performed analysis of the procedure applied on the basis of F48 structure evidences convincingly a clearly exhibited D_3 continuous symmetry of the molecule.

Comparing D_3 symmetry molecule with F48, it is necessary to stress attention on the following. As shown previously, the F48 molecule has been obtained in due course of successive steps of 1,2-additions that strictly keep long-bond framing of the fullerene cage pentagon [66]. Oppositely to this, the exact D_3 symmetry of the isomer requires moving a short bond of the fullerene cage to the pentagon framing. This is possible if only the 1,2-manner of addition is replaced by 1,4-one at the last or one of the preceding steps. A precedent and a possible mechanism for such a spontaneous transformation have not been known so far. On the other hand, geometrical factors given in Table 1 show convincingly that a successive fluorination of the cage did not require any serious reconstruction of the latter which might result in changing the pentagon framing. This means that the main structure factor of the C_{60} cage consisting in the long-single-bond frame of pentagons should be retained during the whole fluorination process since the fluorination of $C_{60}F_2$ to $C_{60}F_{48}$ follows a single pathway and occurs in regular steps.

At the same time, the total energy of the exact D_3-$C_{60}F_{48}$ isomer is significantly lower (about 54 kcal/mol) than that of F48 molecule. It means that under particular kinetic conditions, the formation of more stable isomer might be energetically profitable. “Fluorine dance”, which was discovered ten years ago [67] and was exhibited in a facile migration of fluorine atoms over the fullerene surface at elevated temperature, may obviously provide such particular kinetics. Evidently, the migration itself cannot transform 1,2-addition into 1,4 one. However, if to remember a possible D_{3d} C_{60} isomer [68] (see a detailed discussion of the C_{60} isomerism in Ref. [69]), it seems reasonable to suppose that the fluorine migration alongside with temperature elevating may stimulate reisomerization of the C_{60} cage from C_i and/or I_h form into D_{3d} one, which, in its turn, may favour the formation of D_3 symmetric fluoride. Since experimental recordings related to $C_{60}F_{48}$, such as ^{19}F NMR as well as electronic spectra, etc., depend on a chemical prehistory of samples producing, one might think that both, exact and continuous, D_3-symmetric isomers of the fluoride may coexist shifting balance to one of them depending on chemical and physical treatments.

5.6. $C_{60}F_{50}$–$C_{60}F_{60}$ adducts

Because N_D has been completely worked out by this stage (see Fig. 6), the N_{DA} pointer could not be used and further fluorination had to proceed without it. The problem is facilitated by a comparatively small number of empty places, which decreases when fluorination proceeds, and the isomer study can therefore be performed just routinely by running over all places one by one. The result of the sorting thus performed is presented in Table 1 and in Fig. 11, which shows the structure of the species of the lowest total energy. The fluorination process is ended by the formation of $C_{60}F_{60}$ species of the I_h symmetry. Because there are no odd electrons in the species, its atoms form an ideal truncated icosahedron structure, in contrast to pristine C_{60}, where odd electron conjugation violates the high symmetry lowering it to C_i [26, 60]. When the odd electron behavior is not taken into account, as is the case with close-shell calculations, both RHF and DFT, the C_{60} exact symmetry is obviously I_h. All the above high-fluorinated products are thermodynamically stable and could exist. But because fluorination is a successive process, their formation becomes energetically nonprofitable at $k \geq 25$ due to positive partial coupling energy (see Fig. 6); that is why no recording of the species production has been known by now.

5.7. Fluorination-induced C_{60} cage structure transformation

Stepwise fluorination is followed by the gradual substitution of sp^2-configured carbon atoms by sp^3 ones. Because both valence angles between the corresponding C–C bonds and the bond lengths are noticeably different in the two cases, the structure of the fullerene cage becomes pronouncedly distorted. Figure 12 demonstrates the transformation of the cage structure in the course of fluorination exemplified by changes within a fixed set of C–C bonds.

A gray curve in each panel in Fig. 12 presents the bond length distribution for pristine C_{60}. As seen from the figure, the first steps of fluorination are followed by the elongation of C–C bonds that involve not only the newly formed sp^3 atoms but also some of sp^2 ones. This

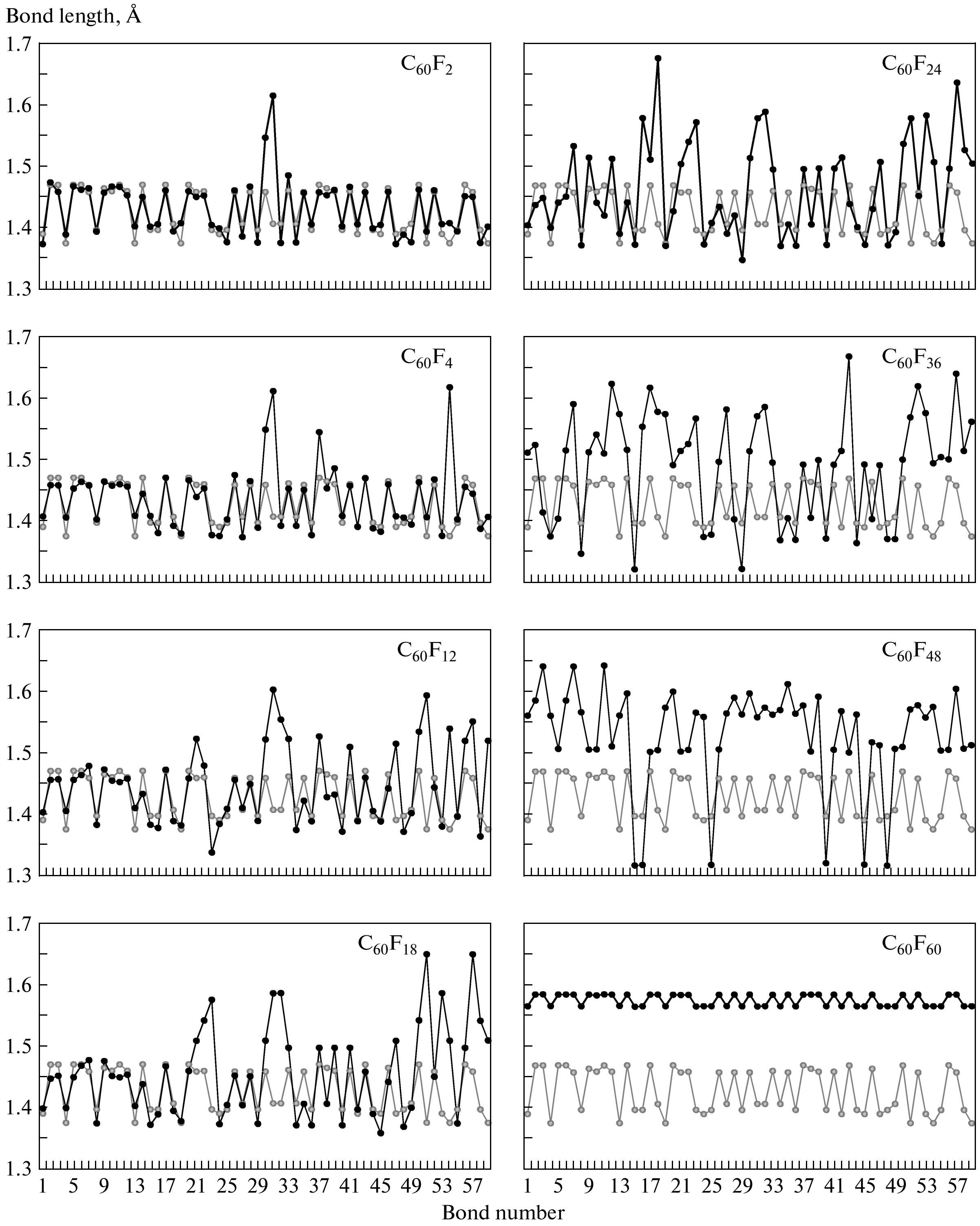

Fig. 12. sp^2-sp^3 transformation of the C_{60} cage structure in the course of successive fluorination. Gray and black curves respectively correspond to the bond length distribution related to the C_{60} cage of pristine fullerene and its fluorinated derivatives

results in an increase in the total number of effectively unpaired electrons N_D, as is shown in Fig. 6. The increase proceeds until $C_{60}F_8$ is formed, after which the effect is compensated by a gradual decrease in the N_D value caused by the increasing number of sp^3 atoms.

Comparing the pristine diagram with those belonging to a current fluorinated species makes it possible to trace the fullerene cage structure changes. As might be naturally expected, the sp^2–sp^3 transformation causes the appearance of elongated C–C bonds, whose number increases as fluorination proceeds. To keep the cage structure closed, this effect as well as changes in valence angles should be compensated. At the level of bonds, this compensation causes the squeezing of a major part of pristine bonds, both long and short, and the squeezing effect grows as fluorination proceeds. This is particularly well seen in the right-hand panels of Fig. 12 related to k-high fluorides where a number of extremely short C–C bonds 1.325–1.320 Å in length are formed. The existence of these bonds is proved experimentally [70]. These six bonds are the only ones that remain untreated in $C_{60}F_{48}$ species and carry information about the pristine structure. Once each of them has been treated as the fluorination proceeds from $C_{60}F_{48}$ to $C_{60}F_{60}$, a new nonstressed cage of the I_h symmetry is formed. It is important to note that although all carbon atoms become sp^3-configured and should be considered fully identical, the short-and-long bond pattern of pristine C_{60} is kept for $C_{60}F_{60}$ as well, although with less difference between the two kinds of bonds. Moreover, the previously short (long) bonds of C_{60} retain their character in $C_{60}F_{60}$. A similar sp^2–sp^3 transformation of the cage was observed under hydrogenation from C_{60} to $C_{60}H_{60}$ [28].

6. CONCLUSION

The reactions of fullerene C_{60} with molecular fluorine have been studied using unrestricted broken symmetry HF semiempirical calculations (the UBS HF version of the AM1 technique of the CLUSTER-Z1 codes). The calculations are focused on a sequential addition of fluorine atoms to the fullerene cage. A complete family of species $C_{60}F_{2k}$ (k = 1–30) has been produced. Based on the concept of effectively unpaired electrons for the selectivity of the fullerene molecule chemical activity as well as on a suggested methodology of a computational synthesis of fullerene derivatives, the quantum-chemical computational synthesis of the above derivatives has been performed following the laboratory synthetic pathway of the relevant reactions in the gaseous state. The preferred binding sites for sequential additions were selected by the largest value of the atomic chemical susceptibility quantified by the fraction of effectively unpaired electrons N_{DA} on the selected atom A. As shown, any addition of fluorine atom causes a remarkable change in the N_{DA} distribution over the C_{60} cage atoms. That is why the synthesis has been performed as a series of predicted sequential steps. Briefly, the synthetic scheme is as follows. The reaction starts around a pair of fullerene C_{60} atoms with the largest N_{DA} values. The atoms usually form one of short-length bonds within one of the six identical naphthalene-core fragments. When the first adduct $C_{60}F_2$ is formed, the reaction proceeds around a new pair of its fullerene cage atoms with the highest N_{DA} values, resulting in the formation of a $C_{60}F_4$ adduct. A new N_{DA} map reveals the sites for the next addition step, and so on. The reaction is terminated when all the N_{DA} values are fully exhausted. Following this methodology, a complete series of $C_{60}F_{2k}$ species has been synthesized. The obtained results are analyzed from the energetic, symmetry, and composition abundance standpoints. A good fitting of the data to experimental findings convincingly proves a creative role of the suggested synthetic methodology in considering fullerene-involved addition reactions of different kinds.

The author is deeply thankful to R. Papoular for performing the Rietveld refining of his high-resolution X-ray data on the $C_{60}F_{48}$ crystal based on author's results and giving permission for publishing the result here.

REFERENCES

1. J. H. Holloway and E. G. Hope, in *The Chemistry of Fullerenes*, ed. by R. Taylor, World Sci., Singapore (1995), p. 109.
2. O. V. Boltalina, J. Fluorine Chem. **101**, 273 (2000).
3. O. V. Boltalina and N. A. Galeva, Uspekhi Khimii **69**, 661 (2000).
4. R. Taylor, Chem. Eur. J. **7**, 4075 (2001).
5. R. L. Jaffe, J. Phys. Chem. B **107**, 10378 (2003).
6. R. Taylor, J. Fluorine Chem. **125**, 359 (2004).
7. K. Balasubramania, Chem. Phys. Lett. **182**, 257 (1991).
8. P. J. Krusic, E. Wasserman, P. N. Keizer et al., Science **254**, 1183 (1991).

9. R. Mitsumoto, T. Araki, E. Ito et al., J. Phys. Chem. A **102**, 552 (1998).

10. N. Matsuzawa, T. Fukunaga, and D. A. Dixon, J. Phys. Chem. **96**, 10747 (1992).

11. B. W. Clare and D. L. Kepert, Mol. Struct. (THEOCHEM) **303**, 1 (1994).

12. A. D. Darwish, A. G. Avent, R. Taylor, and D. R. M. Walton, J. Chem. Soc., Perkin Trans. **2**, 2051 (1996).

13. B. W. Clare and D. L. Kepert, Mol. Struct. (THEOCHEM) **389**, 97 (1997).

14. B. W. Clare and D. L. Kepert, Mol. Struct. (THEOCHEM) **466**, 177 (1996).

15. B. W. Clare and D. L. Kepert, Mol. Struct. (THEOCHEM) **589–590**, 195 (2002).

16. B. W. Clare and D. L. Kepert, Mol. Struct. (THEOCHEM) **589–590**, 209 (2002).

17. A. A. Gakh and A. A. Tuinmann, Tetrahedron Lett. **42**, 7133 (2001).

18. O. V. Boltalina, V. Yu. Markov, R. Taylor, and M. P. Waugh, Chem. Comm. 2549 (1996).

19. O. V. Boltalina, J. M. Street, and R. Taylor, J. Chem. Soc., Perkin Trans. **2**, 649 (1998).

20. A. A. Gakh, A. A. Tuinmann, J. L. Adcock et al., J. Amer. Chem. Soc. **116**, 819 (1994).

21. O. V. Boltalina, L. N. Sidorov, V. F. Bagryantsev et al., J. Chem. Soc., Perkin Trans. **2**, 2275 (1996).

22. E. F. Sheka, in *Lecture Notes in Computer Science, Computational Science — ICCS2003*, Pt. II, ed. by P. M. A. Sloot, D. Abramson, A. V. Bogdanov et al., Springer, Berlin (2003), pp. 386–394.

23. E. F. Sheka, Centr. Eur. J. Phys. **2**, 160 (2004).

24. E. F. Sheka, Int. J. Quant. Chem. **100**, 375 (2004).

25. E. F. Sheka and V. A. Zayets, Zh. Fiz. Khimii **79**, 2250 (2005).

26. E. F. Sheka, Int. J. Quant. Chem. **107**, 2361 (2007).

27. E. F. Sheka, J. Struct. Chem. **47**, 593 (2006).

28. E. F. Sheka, arXiv:0906.2443v1 [cond-mat.mes-hall].

29. N. P. Evlampieva and E. F. Sheka, Full. Nanotubes Carbon Nanostr. **14**, 343 (2006).

30. A. Szabo and N. S. Ostlund, *Modern Quantum Chemistry*, McGraw-Hill, New York (1989), Secs. 3.8.5–3.8.7.

31. K. B. Wiberg, Tetrahedron **24**, 1083 (1968).

32. S. G. Semenov, in *Evolution of the Valence Doctrine* (in Russian), Khimia, Moscow (1977), pp. 148–161.

33. E. F. Sheka and L. A. Chernozatonskii, J. Phys. Chem. C **111**, 10771 (2007).

34. J. Hachmann, J. J. Dorando, M. Aviles, and G. K. Chan, J. Chem. Phys. **127**, 134309 (2007).

35. E. F. Sheka and L. A. Chernozatonskii, Int. J. Quant. Chem. **110**, № 1 (2010).

36. E. F. Sheka and L. A. Chernozatonskii, arXiv: 0901.3229v1 [cond-mat.mtrl-sci].

37. E. R. Davidson and A. E. Clark, Phys. Chem. Chem. Phys. **9**, 1881 (2007).

38. L. Noodleman, J. Chem. Phys. **74**, 5737 (1981).

39. J. A. Pople and R. K. Nesbet, J. Chem. Phys. **22**, 571 (1954).

40. U. Von Barth and L. Hedin, J. Phys. C **5**, 1629 (1972).

41. S. Dutta, S. Lakshmi, and S. K. Pati, Phys. Rev. B **77**, 073412 (2008).

42. V. N. Staroverov and E. R. Davidson, Chem. Phys. Lett. **330**, 161 (2000).

43. K. Takatsuka, T. Fueno, and K. Yamaguchi, Theor. Chim. Acta. **48**, 175 (1978).

44. I. Kaplan, Int. J. Quant. Chem. **107**, 2595 (2007).

45. D. A. Zhogolev and V. B. Volkov, *Methods, Algorithms and Programs for Quantum-Chemical Calculations of Molecules* (in Russian), Naukova Dumka, Kiev (1976), pp. 31–37.

46. P. K. Berzigiyarov, V. A. Zayets, I. Ya. Ginzburg, V. F. Razumov, and E. F. Sheka, Int. J. Quant. Chem. **88**, 449 (2002).

47. K. M. Rogers and P. W. Fowler, Chem. Comm. 2357 (1999).

48. O. V. Boltalina, A. Yu. Lukonin, J. M. Street, and R. Taylor, Chem. Comm. 1601 (2000).

49. O. V. Boltalina, A. D. Darwish, J. M. Street et al., J. Chem. Soc., Perkin Trans. **2**, 251 (2002).

50. O. V. Boltalina, V. Yu. Markov, R. Taylor, and M. P. Waugh, Chem. Comm. 2549 (1996).

51. I. S. Neretin, K. A. Lyssenko, M. Yu. Antipin et al., Angew. Chem. **112**, 3411 (2000).

52. O. V. Boltalina, M. Bühl, A. Khong et al., J. Chem. Soc., Perkin Trans. **2**, 1475 (1999).

53. O. V. Boltalina, A. Yu. Borschevskii, L. N. Sidorov et al., Chem. Comm. 529 (1996).

54. L. G. Bulusheva, A. V. Okotrub, A. A. Shnitov et al., J. Chem. Phys. **130**, 014704 (2009).

55. O. V. Boltalina, J. M. Street, and R. Taylor, J. Chem. Soc., Perkin Trans. **2**, 649 (1998).

56. A. Popov, V. M. Senyavin, O. V. Boltalina et al., J. Phys. Chem. A **110**, 8645 (2006).

57. S. Kawasaki, T. Aketa, H. Touhara et al., J. Phys. Chem. B **103**, 1223 (1999).

58. H. Zabrodski, S. Peleg, and D. Avnir, J. Amer. Chem. Soc. **114**, 7843 (1992).

59. S. Grimme, Chem. Phys. Lett. **297**, 15 (1998).

60. E. F. Sheka, B. S. Razbirin, E. A. Nikitina, and D. K. Nelson, arXiv:1005.1829 [cond-mat.mtrl-sci].

61. A. A. Gakh, A. A. Tuinmann, and J. L. Adcock, J. Amer. Chem. Soc. **116**, 819 (1994).

62. O. V. Boltalina, L. N. Sidorov, V. F. Bagryantsev et al., J. Chem. Soc., Perkin Trans. **2**, 2275 (1996).

63. L. Hedberg, K. Hedberg, O. V. Boltalina et al., J. Phys. Chem. A **108**, 4731 (2004).

64. R. J. Papoular, H. Allouchi, A. V. Dzyabchenko et al., Full. Nanotubes Carb. Nanostr. **14**, 279 (2006).

65. R. J. Papoular, Private investigation.

66. L. Hedberg, K. Hedberg, D. S. Betune et al., Science **254**, 410 (1991).

67. A. A. Gakh and A. A. Tuinman, Tetrahedron Lett. **42**, 7137 (2001).

68. F. N. Tomilin, P. V. Avramov, S. A. Varganov et al., Fiz. Tverdogo Tela **43**, 936 (2001).

69. E. F. Sheka, *Nanoscience of Fullerenes*: *Nanochemistry, Nanomedicine, Nanophotonics, Nanomagnetism*, Taylor and Francis, Boca Raton (2010), in press.

70. S. I. Troyanov, P. A. Troshin, O. V. Boltalina et al., Angew. Chem. Int. Ed. **40**, 2285 (2001).